Dyes and Pigments 95 (2012) 338–343

Contents lists available at SciVerse ScienceDirect

Dyes and Pigments

journal homepage: www.elsevier.com/locate/dyepig

A core-shell silica nanosphere for the off–on chemosensor of iron(III) ions and the targeted probe for optical imaging on HeLa cells

Gen-Ping Tao, Qiu-Yun Chen*, Xia Yang, Kai-Ya Wang

School of Chemistry and Chemical Engineering, Jiangsu University, Zhenjiang 212013, PR China

ARTICLE INFO

Article history:
Received 18 August 2011
Received in revised form
26 March 2012
Accepted 29 April 2012
Available online 19 May 2012

Keywords:
Core-shell
Nanoparticles
Fe(III) ions
Chemosensor
Imaging
Cancer

ABSTRACT

Rhodamine B isothiocyanate doped silica-coated (RBITC-SiO_2) silica nanoparticles were used as three-dimensional scaffolds for fluorophore organization. Di(2-propylcarboxyl)amine (–NH–COOH) groups were conjugated onto the surface of the RBITC@SiO_2 forming a stable water soluble nanospheres (RBITC@SiO_2–NH–COOH), which could sensitize Fe^{3+} ions selectively. State fluorescence measurements allowed us to observe the occurrence of an efficient energy transfer process from coordinated Fe^{3+} ions to the hosted RBITC resulting the turn-off of the emission of RBITC@SiO_2–NH–COOH in water solution. Furthermore, the nanosphere (RBITC@SiO_2–NH–COOH) displays enhanced HeLa cells fluorescence imaging *in vitro* suggesting selective cancer cell payload delivery. It represents a class of novel multi-functional nanoparticles that combines the advantages of active cancer-targeting, compatibility with fluorescence imaging and chemosensors of Fe^{3+} ions.

1. Introduction

The design and development of highly sensitive and specific probes for various metal ions have been a subject of intense interest because of their potential applications in clinical biochemistry and environmental science [1–6]. Metal ion fluorescent probes have been arisen more and more attention because of it extensive use in the environment and biochemistry [7,8]. The detection of trace elements implicated in biological events as well as in environmental issues is still a great challenge and requires selective sensors [9]. Iron(II/III) is an essential metal ion in cells, being present in the structure of many enzymes and proteins and therefore essential for cellular metabolism [10]. And also, most of the process of the cellular level's biology and chemistry need iron(II) to participate [11,12]. Therefore, fluorescent probes of iron(II/III) ions are meaningful to the environment and life science.

The classical design of a fluorescent sensor for metal-ion detection includes two moieties; a receptor responsible for the molecular recognition of the analyte and a fluorophore responsible for signaling the recognition event [13,14]. Recently, silica core-shell fluorescent nanoparticles were widely used as biosensors and probes for optical images [15,16]. Silica has several advantages including its ease of preparation through the hydrolysis–condensation reaction from relatively inexpensive precursor molecules such as tetraethyl orthosilicate (TEOS) in the presence of acid- or base-catalysts, the possibility of surface modification with various well-studied organosilicon compounds, and its non-acute toxicity. To improve the application of silica nanoparticles in biological research, fluorescent dye molecules were introduced into silica nanoparticles using a thiourea-linkage forming reaction through amino-terminated alkyltrialkoxysilane compounds such as (3-aminopropyl)triethoxysilane (APS) and dye molecules having an isothiocyanate functional group, i.e. rhodamine isothiocyanate (RBITC) and fluorescein isothiocyanate (FITC) [16–18]. In the previous report, we found that the di(picolyl)amine (dpa) modified core-shell RBITC@SiO_2–dpa nanoparticles can bind Fe(III) ion forming RBITC@SiO_2–dpa–Fe(III) nanospheres, which could image cancer cell [17]. In this paper, we use silica nanoparticles as three-dimensional scaffolds for fluorophore organization, and di(2-propylcarboxyl)amine groups were conjugated onto the surface of the RBITC@SiO_2 forming a new nanosphere RBITC@SiO_2–NH–COOH, which could sensitize Fe(III) ion, resulting the energy transfer between the modified Fe(III) complex and hosted dyes. We also show the results of imaging cancer cell targeting using di(2-propylcarboxyl)amine modified nanospheres.

* Corresponding author. Tel.: +86 0511 8879800; fax: +86 0511 88791602.
E-mail address: chenqy311@126.com (Q.-Y. Chen).

0143-7208/$ – see front matter © 2012 Elsevier Ltd. All rights reserved.
doi:10.1016/j.dyepig.2012.04.023

2. Materials and methods

2.1. Reagents

Rhodamine B isothiocyanate, Triton X-100, 3-aminopropyltrimethoxysilane (APS), Ethanol, Ethyl 2-bromopropanoate, and solvents were of analytical grade. Rhodamine B isothiocyanate doped silica-coated fluorescent nanoparticles (RBITC-SiO_2) were synthesized as reported [17]. Water was purified with a Millipore Milli-Q system (25 °C:18.2 MΩ cm, 7.20×10^{-2} N/m).

2.2. Apparatus

FT-IR characterizations were performed using a Nicolet Nexus 470 FT-IR spectrophotometer in the spectral range of 4000–400 cm^{-1}. The electronic absorption spectrum was recorded using a UV-2450 UV–Vis spectrophotometer at room temperature. Photoluminescent emission spectra were measured on a American's Varian Carry Eclipse spectrofluorometer. TEM was performed at room temperature on a JEOL JEM-200CX transmission electron microscope using an accelerating voltage of 200 kV. Mean diameter and size distribution of the nanoparticles were measured by dynamic light scattering (DLS) using a Brookhaven 90 plus particle size analyzer. The surface charge of the nanoparticles was investigated through zeta potentials measurements (Nano-Z, Malvern Instruments). The content of carboxyl groups in the nanoparticles was measured by TG-thermogravimetric analyzer (Germany, NETZSCH STA 449C).

2.3. Preparation of nanoparticles

2.3.1. Preparation of the RBITC@SiO_2–NH–COOET

A solution of 0.8075 g APS and 0.7402 g triethylamine and 1.3265 g ethyl 2-bromopropanoate was allowed to reflux 24 h under a nitrogen atmosphere. After the reaction, the solution was obtained by centrifugation. Next, 1.016 g RBITC-SiO_2 were dispersed by sonication in CH_2Cl_2 (15 ml). All the mixed solution was allowed to reflux 24 h. The nanoparticles were isolated by adding acetone (10 ml), washed with ethanol and dried in vacuum at 60 °C for overnight.

2.3.2. Preparation of the RBITC@SiO_2–NH–COOH

Nanoparticles (RBITC@SiO_2–NH–COOET) (50 mg) was dispersed in water (15 ml) and the pH was adjusted at 9–10 with 5% NaOH. The solution was stirred at 70 °C for 1 h, then adjusted the pH to 4–5 with 5% HCl. Nanoparticles were isolated by adding ethanol (20 ml), and dried in vacuum at 60 °C for overnight.

2.4. Cellular uptake and imaging

Human cancer cell line HeLa was obtained from Cancer Cell Repository (Shanghai cell bank). Cells were maintained in RPMI-1640 medium and DMEM medium (Gibco, USA) supplemented with 10% (v/v) heat-inactivated fetal bovine serum, antibiotics (100 U/ml penicillin and 100 U/ml streptomycin), at 37 °C in a humidified atmosphere of 5% CO_2. HeLa cells (2.4×10^4) were seeded into 24-well plates (Every plate was 100 μl) and cultured for 24 h, then nanoparticles (test nanoparticles (2.0 mg) were dispersed in H_2O and diluted with culture media) were added and incubated for 3 h. At last, cells were washed with PBS twice to remove the free nanoparticles. Nanoparticles uptake and imaging of HeLa cells were observed using Nikon Ti-E2000 microscope with live cell system (LCS) which can provide CO_2, temperature control and position fixing. The bright and fluorescence imaging of cells (ex. 555 nm) were recorded and analyzed.

3. Results and discussions

3.1. Characterization

Di(2-propylcarboxyl)amine (–NH–COOH) groups were conjugated onto the surface of the RBITC@SiO_2 forming a water soluble nanospheres (RBITC@SiO_2-NH-COOH) (Scheme 1).FT-IR spectra of the RBITC@SiO_2–NH–COOET silica nanospheres confirmed the existence of ester groups with characteristic peaks around at 1749 and 1164 cm^{-1} that correspond to stretching bands of C=O and C–O–C, respectively. The peak at 2990 cm^{-1} belongs to the stretching bands C–H. The strong peaks around at 1101 cm^{-1} also confirmed the existence of SiO_2 which corresponds to stretching band of Si–O. The disappearance of the peaks around at 1749 cm^{-1} or the appearance of the peak at 1456 cm^{-1} indicates the formation of RBITC@SiO_2–NH–COOH (Fig. 1).

The bands at 211 nm belong to the π–π^* transition bands (Fig. 2). 555 nm of π–π^* transition bands belongs to rhodamine B isothiocyanate. The emission bands at 582 nm of RBITC@SiO_2–NH–COOH show that the surface modified groups had a little influence on the fluorescence emission of RBITC.

The size of nanospheres was measured with a Hitachi-800 transmission electron microscope. The results from TEM showed that the size of nanoparticles RBITC-SiO_2 was 80 ± 5 nm and were uniform (Fig. 3a). The diameter of nanospheres RBITC@SiO_2–NH–COOEt and RBITC@SiO_2–NH–COOH were in the range of 150–170 nm and 15–20 nm, respectively (Fig. 3band c), and the modified nanoparticles RBITC@SiO_2–NH–COOH was highly dispersible in ethanol. Dynamic light scattering (DLS) measurements showed that the core-shell RBITC@SiO_2–NH–COOH had a average hydrodynamic size of 15 nm (Fig. 4), which was much smaller than that of RBITC@SiO_2–NH–COOET (150–170 nm). The surface charge of RBITC@SiO_2–NH–COOET and RBITC@SiO_2–NH–COOH in ethanol solution is −2.51 mV and 2.32 mV, respectively.

TGA measurements have been conducted for RBITC@SiO_2–NH–COOEt and RBITC@SiO_2–NH–COOH. These results are shown as Fig. 5. The thermal decomposition of RBITC@SiO_2–NH–COOEt proceeds with four decomposition steps. A 1.25% weight loss in 0–150 °C indicates the existence of surface adsorbed water molecules. The 30.32% weight loss in 150–245 °C is assigned to the loss of oxethyl groups, further loss of 32.18% in 245–455 °C ascribes to the loss of propionyloxy groups and a 5.4% weight loss in 245–746 °C is assigned to the loss of the aminopropyl

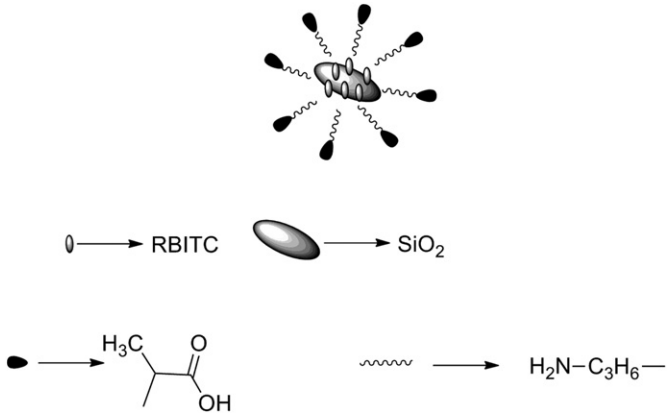

Scheme 1. The RBITC@SiO_2–NH–COOH.

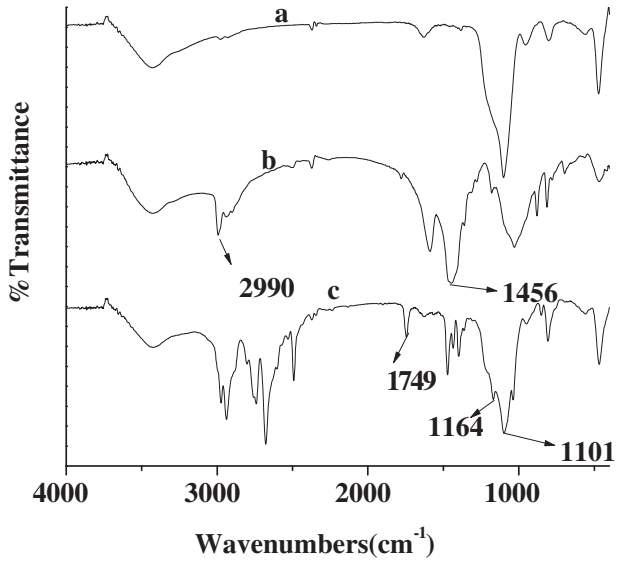

Fig. 1. IR spectral. a. RBITC@SiO_2, b. RBITC@SiO_2–NH–COOH, c. RBITC@SiO_2–NH–COOEt.

groups. The first step for the RBITC@SiO_2–NH–COOH falls in the range of in 185–327 °C with the 14.89% weight loss, which is assigned to the loss of carboxylic groups, confirming the existence of surface-modified carboxylic groups. The 9.37% weight loss in 327–514 °C is assigned to the loss of propionyloxy groups, further loss of 52.97% in 514–963 °C ascribes to the loss of the silicon dioxide shell's triethoxysilane. The thermal decomposition data obtained supports the existence of two nanoparticles.

3.2. Fluorescent properties

The emission wavelengths from the fluorescent silica nanoparticles are similar to those of the parent dye molecules and silica nanoparticles in the aqueous solution producing a very bright photoluminescence. The Si–OH groups on the surface of silica nanoparticles were successfully modified with $-N(CH_2(CH_3)COOH)_2$ enhancing the biocompatibility and sensitivity to transition metal ions. The effect of transition metal ion on the fluorescence of the RBITC@SiO_2–NH–COOH was shown in Fig. 6. It is found that the fluorescence intensity gradually decreased as the concentration of Fe^{3+} increased. The fluorescence of RBITC@SiO_2–NH–COOH (0.028 mg/ml) in water solution was quenched completely when Fe^{3+} ions (42 μM) were added, which is different from our previous reported RBITC@SiO_2–dpa–Fe(III) nanospheres [17]. It was reported that Fe^{3+} ions could induce the

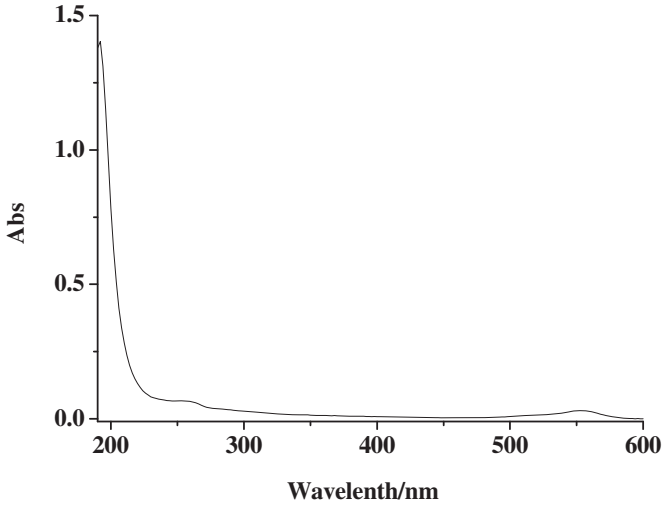

Fig. 2. UV spectral of RBITC@SiO_2–NH–COOH (1.6 mg) dispersed in water (10 ml).

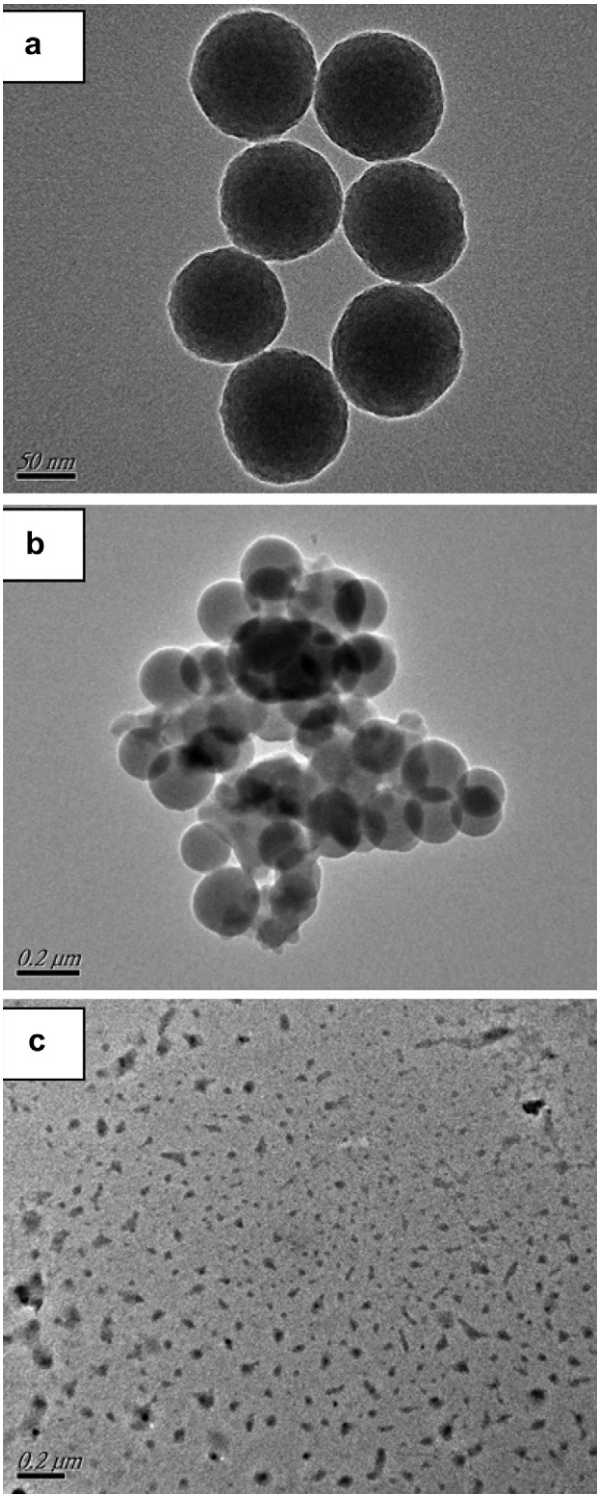

Fig. 3. Transmission electron micrographs of (a) RBITC@SiO_2 (b) RBITC@-SiO_2–NH–COOEt (c) RBITC@SiO_2–NH–COOH.

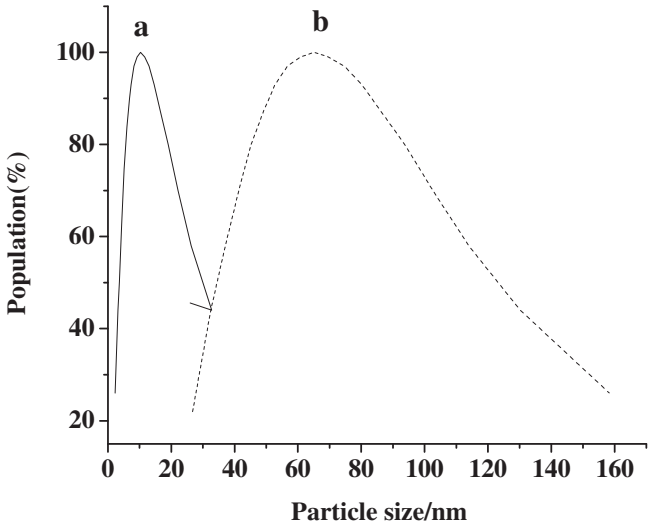

Fig. 4. Size distribution of RBITC@SiO_2–NH–COOH (a) and RBITC@SiO_2 (b) in water.

ring open of the non-fluorescent spirocyclic forms of rhodamine derivatives giving a fluorescent "on" signal [18,19]. However, comparing experimental results showed that there was no obvious change for the emission of RBITC@SiO_2 when Fe^{3+} was added. These indicated that there was no direct interaction between Fe^{3+}

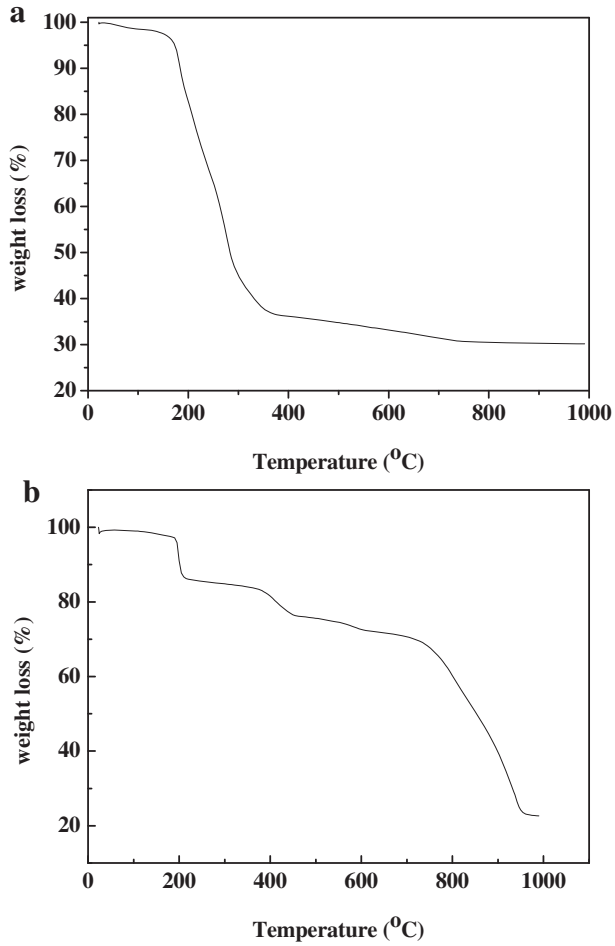

Fig. 5. TG curves of RBITC@SiO_2@–NH–COOEt (a); RBITC@SiO_2@ –NH–COOH (b).

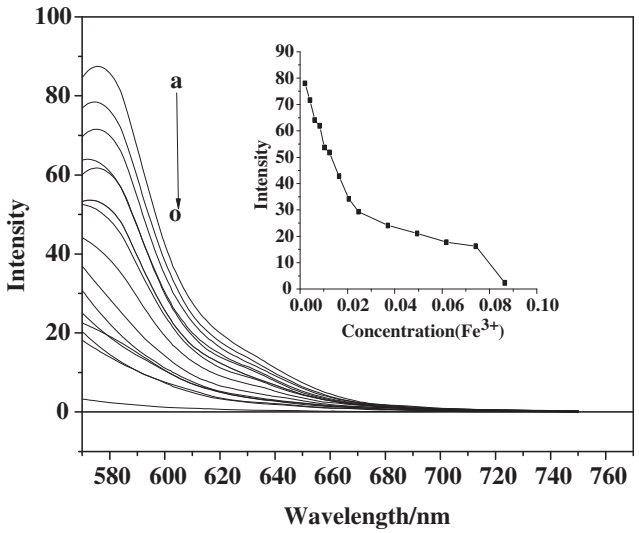

Fig. 6. Emission spectra (excitation at 555 nm) of RBITC@SiO_2–NH–COOH (line a, 0.028 mg/ml) in the presence of Fe^{3+} ($\times 10^{-5}$ M) at pH 7. (a–o: 0, 1, 2, 3, 4, 5, 6, 7, 8, 9, 10, 12, 18, 24, 36, 42). The slit width at the excitation and emission of the spectrofluorimeter is 5. Inset: emission peak intensities versus Fe^{3+} concentration.

and the hosted dyes. The quench effect for Fe^{3+} on the RBITC@SiO_2–NH–COOH was caused possibly by the interaction between surface chelated ferric ions and hosted RBITC in RBITC@SiO_2–NH–COOH giving a "turn-off" signal. The Fe^{3+} is an efficient fluorescence quencher because of its paramagnetic nature [20]. The energy transfer between chelated ferric ions in the shell and RBITC in the core was confirmed by UV spectrum with the enhanced absorption in the range of 200–400 nm, which is similar to the reported energy transfer procedure from silica core-surfactant shell nanoparticles to hosted molecular fluorophores [16]. Other paramagnetic metal ions (Ni^{2+}, Mn^{2+}, Gd^{3+}, Cu^{2+}, Co^{2+}) in the same concentration could not quench the emission of RBITC@SiO_2–COOH (Fig. 7). These indicated that the interaction between surface chelated paramagnetic metal ions and hosted

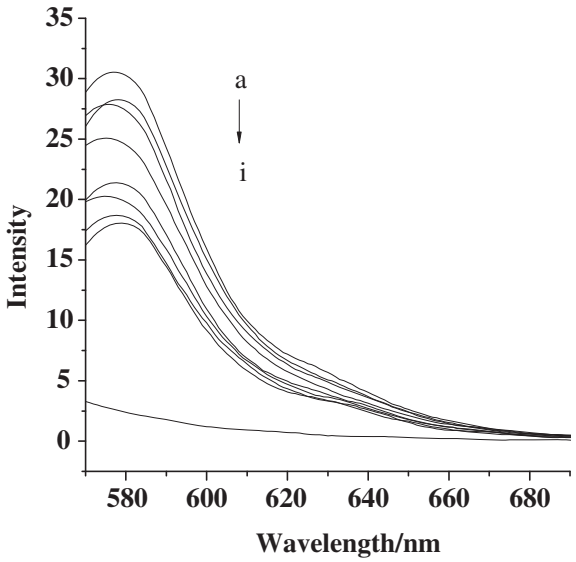

Fig. 7. Emission spectra (excitation at 555 nm) of RBITC@SiO_2–NH–COOH (line a, 0.016 mg/ml) in the presence of various metal ions (4.2×10^{-5} M) at pH 7. (b–i: Zn^{2+}, Ni^{2+}, Mn^{2+}, La^{3+}, Gd^{3+}, Cu^{2+}, Co^{2+}, Fe^{3+}).

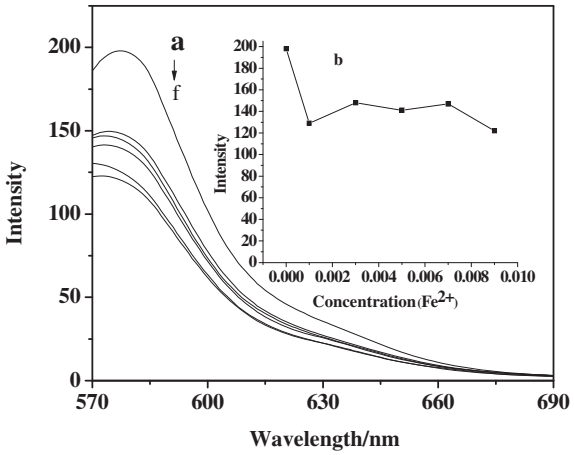

Fig. 8. Emission spectra (excitation at 555 nm) of RBITC@SiO_2–NH–COOH (line a, 0.33 mg/ml) in the presence of (NH_4FeSO_4) ($\times 10^{-5}$ M) at pH 7. (a–f: 0, 1, 3, 5, 7, 9). The slit widths at the excitation and emission of the spectrofluorimeter is 5. Inset: emission peak intensities versus Fe^{2+} concentration.

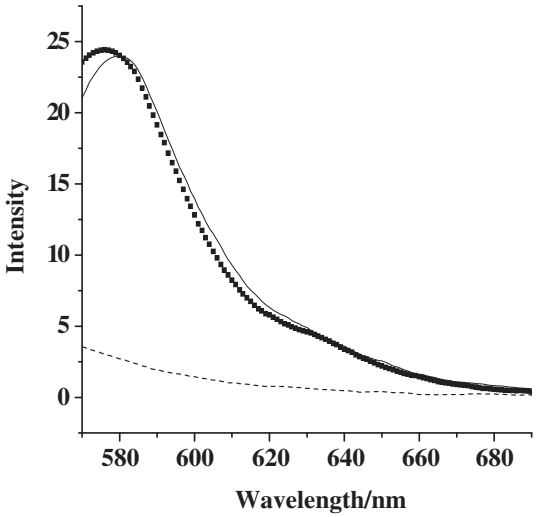

Fig. 9. Emission spectra (excitation at 555 nm) of RBITC@SiO_2–COOH (line (—), 0.015 mg/ml) in the presence of Fe^{3+} (3.9×10^{-5} M, line (- - -)) and EDTA (3.9×10^{-4} M, line (◆)) at tris buffer. The slit width at the excitation and emission of the spectrofluorimeter is 5.

RBITC in the RBITC@SiO_2–NH–COOH was affected possibly by the geometry and stability of RBITC@SiO_2–NH–COOH–M^{n+} ($n = 2,3$) complexes.

The most biologically relevant Fe^{2+} barely perturb the fluorescence of the RBITC@SiO_2–NH–COOH. Addition of 42 μM concentrations of the Fe^{2+} into aqueous solution of RBITC@SiO_2–NH–COOH induces blue-shift about 10 nm of emission (Fig. 8). These properties would possibly make RBITC@SiO_2–NH–COOH of value in measurement of overloaded free Fe^{3+} *in vitro* essay and distinguish Fe^{3+} from Fe^{2+}. The intensity and emission wavelength of the RBITC@SiO_2–NH–COOH in solution were not significantly affected by the changes of pH, as confirmed by the strong emission at 560 nm in aqueous solution at pH 4–9, indicating that nanoparticles are stable in aqueous solution. So RBITC@SiO_2–NH–COOH can be regarded as a Fe(III) ions chemosensor. Because EDTA has stronger complexation with ferric ions, it could be used for de-complexation of RBITC@SiO_2–NH–COOH–Fe^{3+}. The quenched fluorescence could be recovered when an equal amount of EDTA was added (Fig. 9). So, RBITC@SiO_2–NH–COOH can be used as off–on fluorescence sensor for the Fe^{3+} (quencher) and EDTA (recovering reagent).

3.3. Cell uptake and imaging

The fluorescence image of the RBITC@SiO_2–NH–COOH was assayed using HeLa cells. For HeLa cells treated with RBITC-SiO_2, the observed red fluorescence image indicates that these nanoparticles were located outside of HeLa cells due to the relative larger size and low water solubility, which resulted in no internalization of the non-targeted control. In contrast, the intense cellular fluorescence was observed when HeLa cells were incubated with the RBITC@SiO_2–NH–COOH (Fig. 10). Nearly all the cells displayed the RBITC signal. All emissions from the nanoparticle-containing culture medium surrounding the cells were removed by washing the cells with PBS. Electron micrographs of the cells provided direct evidence that a large number of RBITC@SiO_2–NH–COOH were endocytosed by HeLa cells. The mitochondrial membrane potentials of tumor cells were higher than those of normal cells, most agents have a positively charged moiety that take advantage of electrostatic forces in locating its target [21]. These preliminary data revealed that the targeting ability of nanospheres to HeLa cells was enhanced greatly due to the di(2-propylcarboxyl)amino groups conjugated onto the surface of the RBITC@SiO_2 allowing cellular uptake through intracellular passive accumulation and mitochondrial membrane of cancer cells induced accumulation.

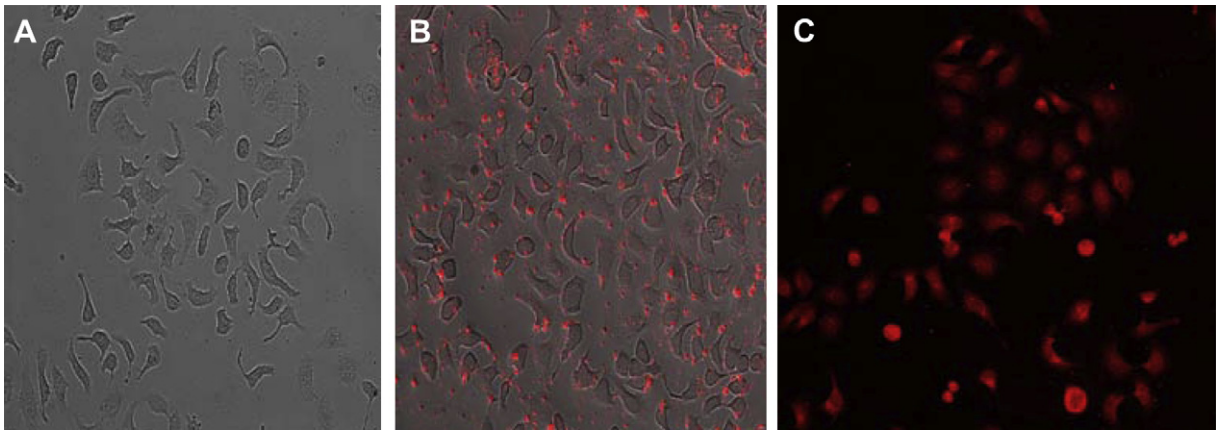

Fig. 10. Fluorescence images of HeLa cells treated with nanoparticles (2.0 mg) and incubated for 3 h. A, control; B, RBITC-SiO_2; C, RBITC@SiO_2–NH–COOH.

4. Conclusion

A water soluble stable core-shell nanoparticles RBITC@SiO_2–NH–COOH showed enhanced fluorescence imaging of HeLa cells, indicating that it can target cancer cells through intracellular passive accumulation and mitochondrial membrane of cancer cells accumulation *in vitro* for fluorescence images. It is interesting to find that Fe^{3+} ions can selectively quench the emission of fluorescence core-shell nanoparticles (RBITC@SiO_2–NH–COOH). So RBITC@SiO_2–NH–COOH could be used as a multifunctional nano-material that enables simultaneous imaging and chemosensors of Fe^{3+} ions, which is different from traditional non-aqueous chemosensors of Fe^{3+} ions [22]. These properties would possibly make RBITC@SiO_2–NH–COOH of value in measurement of free Fe^{3+} *in vitro* essay. This crucial observation opens up new perspectives in the design of multifunctional structures based on silica nanoparticles, which could revolutionize the field of nanosensors and nanodevices.

Acknowledgments

Financial support from National Science Foundation of China (20971059) and distinguished scholar science foundation of Jiangsu University (06JDG050).

References

[1] Wu XF, Xu BW, Tong H, Wang LX. Phosphonate-functionalized polyfluorene film sensors for sensitive detection of iron(III) in both organic and aqueous media. Macromolecules 2010;43:8917–23.
[2] Cuesta L, Sessler JL. π-Metal complexes of tetrapyrrolic systems. A novel coordination mode in "porphyrin-like" chemistry. Chemistry Society Review 2009;38:2716–29.
[3] Liu W, Xu L, Sheng R, Wang P, Li HA. Water-soluble "switching on" fluorescent chemosensor of selectivity to Cd^{2+}. Organic Letter 2007;9:3829–32.
[4] Ando S, Koide K. Development and applications of fluorogenic probes for mercury(II) based on vinyl ether oxymercuration. Journal American Chemical Society 2011;133:2556–66.
[5] Kramer R. Fluorescent chemosensors for Cu^{2+} ions: fast, selective and highly sensitive. Angewandte Chemie International Edition 1998;37:772–3.
[6] Xiao WX, Xiao D, Xia JH, Chen ZC. Fluorescent sensing of nitrite at nanomolar level using functionalized mesoporous silica. Microchim Acta 2011;173:73–8.
[7] Zhang MC, Sheng YL. An indirect competitive fluorescence immunoassay for determination of dicyclohexyl phthalate in water samples. Journal Fluorescence 2010;20:1167–73.
[8] Majzoub AB, Cadiou C, Dechamps-Olivier I, Tinant B, Chuburu F. Cyclam-methylbenzimidazole: a selective off–on fluorescent sensor for zinc. Inorganic Chemistry 2011;50:4029–38.
[9] Ravikumar I, Ghosh P. Zinc(II) and PPi selective fluorescence off–on–off functionality of a chemosensor in physiological conditions. Inorganic Chemistry 2011;50:4229–31.
[10] Meneghini R. Iron homeostasis, oxidative stress, and DNA damage. Free Radical Biological Medicine 1997;23:783–92.
[11] Aisen P, Wessling Resnick M, Leibold EA. Iron metabolism. Current Opinions on Chemical Biology 1999;3:200–6.
[12] Touati D. Iron and oxidative stress in bacteria. Archives of Biochemistry Biophysics 2000;373:1–6.
[13] Ha SW, Camalier CE, Beck JGR, Lee JK. New method to prepare very stable and biocompatible fluorescent silica nanoparticles. Chemical Communication; 2009:2881–3.
[14] Lv FT, Feng XL, Tang HW, Liu LB, Yang Q, Wang S. Development of film sensors based on conjugated polymers for copper(II) ion detection. Advanced Functional Materials 2011;21:845–50.
[15] Ma YM, Luo W, Quinn PJ, Liu ZD, Hider RC. Design, synthesis, physicochemical properties, and evaluation of novel iron chelators with fluorescent sensors. Journal of Medicinal Chemistry 2004;47:6349–62.
[16] Rampazzo E, Bonacchi S, Juris R, Montalti M, Genovese D, Zaccheroni N, et al. Energy transfer from silica core-surfactant shell nanoparticles to hosted molecular fluorophores. Journal of Physics and Chemistry B 2010;114: 14605–13.
[17] Tao GP, Chen QY, Yang X, Zhao KD, Gao J. Targeting cancer cells through iron(III) complexes of di(picolyl)amine modified silica core-shell nanospheres. Colloids and Surface B: Biointerface 2011;86:106–10.
[18] Chen F, Bu WB, Zhang LX, Fan YC, Shi JL. Is black iron oxide nanoparticle always a light absorber? Journal of Material Chemistry 2011;21:7990–5.
[19] Mao J, Wang NL, Dou W, Tang XL, Yan Y, Liu WS. Tuning the selectivity of two chemosensors to Fe(III) and Cr(III). Organic Letters 2007;9:4567–70.
[20] Xiang Y, Tong AJ. A new rhodamine-based chemosensor exhibiting selective Fe(III)-amplified fluorescence. Organic Letters 2006;8:1549–52.
[21] Chen QY, Zhou DF, Huang J, Guo WJ, Gao J. Synthesis, anticancer activities, interaction with DNA and mitochondria of manganese complexes. Journal of Inorganic Biochemistry 2010;104:1141–9.
[22] Kumar M, Kumar R, Bhalla V. Optical chemosensor for Ag^{+}, Fe^{3+} and cysteine: information processing at molecular level. Organic Letters 2011;13:366–9.